NASA Technical Memorandum 86768

A Three-Dimensional Turbulent Boundary Layer Undergoing Transverse Strain and Streamwise Pressure Gradient

Sheshagiri K. Hebbar and David M. Driver

August 1985

NASA
National Aeronautics and
Space Administration

NASA Technical Memorandum 86768

A Three-Dimensional Turbulent Boundary Layer Undergoing Transverse Strain and Streamwise Pressure Gradient

Sheshagiri K. Hebbar
David M. Driver, Ames Research Center, Moffett Field, California

August 1985

National Aeronautics and
Space Administration

Ames Research Center
Moffett Field, California 94035

This Page Intentionally Left Blank

NOMENCLATURE

C_{fx}	axial (streamwise) skin-friction coefficient = $\tau_{wx}/(1/2)\rho_\infty U_\infty^2$
C_{fz}	peripheral (transverse) skin-friction coefficient = $\tau_{wz}/(1/2)\rho_\infty U_\infty^2$
C_p	pressure coefficient = $(p - P_{ref})/(1/2)\rho_\infty U_\infty^2$
D	diameter of stationary cylinder
h	step height or fence height
L	length of stationary cylinder
P	static pressure
ΔP	pressure difference across fence element
u_τ	friction velocity = $(\tau_w/\rho_\infty)^{1/2}$
U,V,W	mean velocity components in axial, normal, and peripheral directions, respectively
W_s	peripheral velocity on surface of rotating cylinder (spinner)
x,y,z	coordinate system representing axial, normal, and peripheral distances from the start of stationary cylinder (see fig. 1)
α	angle between wall shear-stress vector and normal to fence element
β_w	surface-flow angle (angle between wall shear-stress vector and x-axis), angle between wall shear-stress vector and center line of surface-fence gage
δ	boundary-layer thickness
θ	momentum thickness
ν	molecular kinematic viscosity of air
ρ	density of air
τ_w	total wall shear stress
τ_{wx}, τ_{wz}	axial (streamwise) and peripheral (transverse) wall shear stresses, respectively

Subscripts

L,R	left and right fence elements on directional surface-fence gage, respectively (see fig. 4)
N	normal position of fence element ($\alpha = 0$)
w	wall conditions
∞	free-stream conditions

A THREE-DIMENSIONAL TURBULENT BOUNDARY LAYER UNDERGOING TRANSVERSE STRAIN AND STREAMWISE PRESSURE GRADIENT

Sheshagiri K. Hebbar* and David M. Driver

Ames Research Center

SUMMARY

Results from an experimental investigation designed to provide data on both mean and turbulence quantities in the axisymmetric, swirling boundary layer (with and without pressure gradient) flowing over a stationary cylinder downstream of a spinning cylindrical section are presented. The pressure gradient was introduced into the flow field by a 25.4-mm-high, forward-facing, circular step mounted on the stationary cylinder, the step height being nearly equal to the thickness of the approaching boundary layer. All the measurements were made at a nominal upstream reference Reynolds number of 2.4×10^6/m (corresponding to an upstream reference velocity of 36-37 m/sec) with the rotation of the spinner set to make its peripheral speed equal the reference velocity. The data reported include measurements of surface pressure and the mean surface shear-stress vector taken with a miniature, directional, surface-fence gage. These measurements were supplemented by oil-flow visualization studies of the stationary cylinder. The data indicate that the streamwise pressure gradient controls the development of the streamwise component of wall shear, but leaves the peripheral component of wall shear practically unaffected. Comparison of the data with predictions from a boundary-layer computer code, using a Reynolds-stress equation model and a slightly modified, experimental pressure distribution, shows that it is possible to predict the attached flow field and the location of the separation reasonably well.

INTRODUCTION

In recent years, a considerable amount of work has been done in the area of computational aerodynamics as it is expected to have a significant role in the future development of aerospace vehicles (ref. 1) As the simulation of the dyanmics of turbulence is still difficult to achieve, turbulence modeling remains one of the key pacing items in the development of computer codes for computational aerodynamics. A crucial part of turbulence model development is its evaluation against a wide range of experimental data. In a recent paper, the current status of turbulence modeling for external aerodynamic flows has been reviewed using typical examples to illustrate comparisons between experiments and computations for two- and three-dimensional flows (ref. 2). It has been shown that, for most of the

*Senior NRC Research Associate.

two-dimensional or axisymmetric, attached flows and three-dimensional, attached flows with moderate crossflows (< 15°), modeling based on eddy-viscosity concepts will probably be satisfactory. However, both eddy-viscosity and Reynolds-stress models fail to satisfactorily predict the strongly skewed, three-dimensional flow fields of practical interest to aerodynamicists. These include such flows as boundary layers over swept wings, flows involving wing-body junctions, and axisymmetric, swirling boundary layers. The failure is attributed to the difficulties in the existing boundary-layer approximations and/or turbulence models.

Several investigations of three-dimensional flows have been reported. A critical review of experimental studies in three-dimensional, turbulent boundary layers is given by Johnston (ref. 3). Bissonnette and Mellor (ref. 4) made measurements of mean and turbulence quantities in an axisymmetric, turbulent boundary layer skewed by an axially rotating cylinder. Similar experiments have also been carried out by Furuya et al. (ref. 5) and Arzoumanian et al. (ref. 6). In a recent survey paper, Nakamura and Yamashita (ref. 7) discuss various aspects of the boundary layer which develops on a spinning, axisymmetric body in an axial flow. Elsenaar et al. (ref. 8) studied the flow field of a swept flat plate that was similar to the flow field of a wing of infinite aspect ratio. Reference 9 is a discussion on the experimental study of the near-wall region of a three-dimensional, incompressible, turbulent boundary layer relaxing in a zero pressure gradient. Recently, Fernholz and Vagt (ref. 10) made turbulence measurements in an adverse-pressure-gradient, three-dimensional, turbulent boundary layer along a circular cylinder.

A major program of study related to such three-dimensional flows has been under way at NASA Ames Research Center. One of the goals of this program is to improve the general understanding of three-dimensional, viscous flow fields of practical interest and to assess/improve the applicability of existing turbulence models. Several building block experiments have been carried out in connection with this program. In particular, to provide guidance for modeling the pressure-strain correlations and the low Reynolds number terms in the Reynolds-stress model, Higuchi and Rubesin (ref. 11) recently studied the effects of transverse strain on a shear-driven, axisymmetric, turbulent boundary layer in a zero pressure gradient. Mean measurements were made in the relaxing flow region on a stationary cylinder downstream of a spinning cylindrical section (see ref. 12). The experimental data were compared with predictions based on different pressure-strain correlation models. The main conclusion of this study is that Reynolds-stress modeling seems to have advantages over the eddy-viscosity models and predictions based on it showed better agreement with the experimental data. The question remains as to whether the same conclusion holds under pressure gradient conditions.

The present investigation addresses this question. In particular, the effect of axial pressure gradient on the transverse strain flow in the relaxing boundary layer downstream of the spinning cylindrical section is studied. The flow configuration is the same as that used by Higuchi and Rubesin (ref. 11), except for an induced adverse pressure gradient. This adverse pressure gradient was induced in

the approaching flow field by inserting a circular step[1] (i.e., a collar) on the stationary cylinder. Measurements reported herein include surface-pressure distributions and mean-surface shear stresses (magnitude and direction) obtained using a miniature, directional surface-fence gage. The latter were supplemented by oil-flow visualization studies of the stationary cylinder.

The research was conducted while the first author held a senior National Research Council Research Associateship at the NASA Ames Research Center. The authors wish to express their sincere thanks to Mr. J. G. Marvin and Mr. M. Rubesin for their encouragement and suggestions during the course of this investigation.

FLOW CONFIGURATION AND INSTRUMENTATION

The experimental arrangement is essentially the same as that used in reference 11 and is shown in figure 1. The experiments were carried out in the 305-mm × 305-mm (12-in. × 12-in.) low-speed wind tunnel, which had a 140-mm-(5.5-in.-) diameter circular cylinder mounted along its centerline. A section of the cylinder can be rotated to produce a swirling boundary layer. This section is herein referred to as the "spinner." Free-stream velocities up to 50 m/sec are obtainable in the test section. Large glass side windows allow laser beam access to the tunnel. To facilitate surface measurements, a longitudinal hatch is provided along a side generator of the stationary cylinder. This hatch can be closed with either of the two instrumentation panels; one carrying a series of static-pressure taps and the other a series of instrumentation ports, each 3.2 mm (0.125 in.) in diameter which accommodates a surface-fence gage, surface-heat gage, etc. Pressure gradient was introduced into the flow field by mounting a circular sleeve of suitable thickness on the stationary cylinder to act as a forward-facing, circular step. Three step heights, namely 12.7 mm (0.5 in.), 19 mm (0.75 in.) and 25.4 mm (1 in.), were used for this purpose.

The instrumentation included a miniature, directional, surface-fence gage for wall-shear stress measurement and a three-component laser Doppler velocimeter (LDV) for mean and turbulence measurements in the boundary layer (ref. 13). these measurements were supplemented by static-pressure measurements and oil-flow visualization studies of the stationary cylinder. The overall diameter of the surface-fence gage is 3.2 mm. It has two fence elements arranged in a V-shape with a 90° included angle. Each fence element has a square cross-section 0.064 mm wide and

---

[1]A literature survey and a numerical study were carried out to arrive at this tunnel-model configuration that introduced a pressure gradient into the flow field. The numerical study consisted of obtaining solutions from the spinning version of an existing, turbulent, boundary-layer code. Based on the results of this study and on practical considerations, it was decided to mount a circular step on the stationary cylinder and to investigate the resulting boundary layer ahead of the step.

0.11 mm high, with a 0.102-mm × 0.485-mm pressure tap on either side. Additional detailed constructional and operational features of the miniature, directional, surface-fence gages may be found elsewhere (ref. 14).

The fence elements were calibrated in a zero pressure gradient on the bottom wall of the low-speed tunnel against a 1.6-mm-diameter Preston probe. Figure 2 shows the magnitude calibration of the fence elements in the usual nondimensional coordinates. The slight variations in individual calibration of the elements are attributable to geometrical mismatch between the elements. The straight-line fit represents the data quite well, particularly in the higher range, and is essentially equal to the calibration reported in reference 9. The overall accuracy of the calibration is estimated to be within ±5%. The yaw characteristics of the fence elements are shown in figure 3, where α is the angle between the direction of the wall shear-stress vector and the normal to the fence element. But for small differences between the individual fence data, the directional sensitivities closely follow a cosine law. The directional calibration of the fence gage is presented in the usual form in figure 4, where β_w represents the angle between the direction of the wall shear-stress vector and the gage centerline. In the range $-45° \leq \beta_w \leq +45°$, the data points fall on a 45° straight line. Outside this range, one of the gage elements will be in the wake of the other element and the resulting wake interference causes the data to deviate from the straight line. Therefore, during actual experiments, care was taken to see that the gage was roughly aligned with the local, surface-flow direction to avoid wake-interference effects. The accuracy in the directional calibration is estimated to be ±1°.

The above calibration data refer to zero pressure gradient case and have been used for evaluating data taken with the gage in actual experiments involving pressure gradient. No correction was applied to fence readings for pressure-gradient effect because the estimated pressure difference across the fence element resulting from the pressure gradient was found to be small compared to the fence output.

EXPERIMENTS

All the measurements were made at a nominal, upstream Reynolds number of 2.4×10^6/m corresponding to an upstream velocity of 36-37 m/sec. The rotation of the spinner (i.e., rotating section of the cylinder) was adjusted to make its peripheral speed equal to the upstream reference velocity. Detailed surface measurements were made along a side generator of the stationary cylinder as follows (x is measured downstream from the end of the spinner).

Zero Pressure Gradient (No Step) With and Without Rotation

1. Surface static-pressure measurements on the stationary cylinder were taken with 57 closely spaced pressure taps located on the instrumentation panel in the interval 3.2 mm $\leq x \leq$ 635 mm.

2. Surface shear-stress vector measurement on the stationary cylinder using a miniature, directional, surface-fence gage at x = 6.35, 12.7, 19, 25.4, 38, 76, 89, 101.6, 127, 152.4, 203.2, 304.8, 406.4, 508 and 609.6 mm.

Pressure Gradient (25.4-mm Step at x = 154 mm) With and Without Rotation

1. Surface static-pressure measurements on the stationary cylinder up to the step, i.e., 3.2 mm $\leq x \leq$ 152.4 mm.

2. Surface shear-stress vector measurement on the stationary cylinder up to the step, i.e., at x = 6.35, 12.7, 19, 25.4, 38, 76, 89, 101.6, 127 and 152.4 mm.

RESULTS AND DISCUSSION

As reported by Higuchi and Rubesin (ref. 11), the flow field in the test section was of high quality with a pressure gradient that was nominally zero. The boundary layer developing on the spinner was axisymmetric and was found to be essentially collateral at the end of the spinner. However, as the tunnel was relocated and as some minor modifications were incorporated into the tunnel to further improve the flow quality, it was necessary to check the flow field in the test section. Wall shear-stress measurements were therefore performed with a 1.6-mm-diameter Preston probe at x = -101.6 mm and at intervals of 10° on the circumference of the stationary spinner. Figure 5 shows the distribution of streamwise, skin-friction coefficient values along the circumference of the stationary spinner. A total variation of 9% observed in the distribution of skin-friction coefficient is within the experimental uncertainty of ±5% and the axisymmetry of the wall-shear stress is therefore considered good. However, mean velocity data (ref. 13) indicated a slightly thicker boundary layer at the end of the spinner (nearly 12% thicker than the value quoted by Higuchi and Rubesin).

The experimental data are discussed below (figs. 6-17), with particular emphasis on the effect of the adverse pressure gradient on the transverse strain flow in the boundary layer, and compared with spin-code estimates based on Reynolds-stress modeling. The reduced data are documented in tables 1-6.

Static-Pressure Distribution

Figure 6 shows measured static-pressure distribution on the stationary cylinder (without step) with and without rotation. It also shows the pressure distribution on the tunnel bottom wall. Note that the pressure level inside the test section is slightly below atmospheric, say within ±2% of the free-stream dynamic head. It is

suspected that the small variations of pressure observed near the beginning of the stationary cylinder are caused by the presence of a small lip formed as a result of the mismatch at the junction of the spinner and the stationary cylinder. But for these variations, the data indicate a pressure gradient that was nominally zero over the stationary cylinder. As expected, with rotation, the static pressure on the surface is reduced slightly. This is because a pressure gradient across the boundary layer will exist if there is a swirl flow with transverse curvature.

Three steps of height 12.7 mm, 19 mm and 25.4 mm were available for introducing pressure gradient into the flow field. The approaching, spinning boundary layer (ref. 12) at the end of the spinner was nearly 25 mm thick. At $x = 3.2$ mm from the spinner, the surface-flow angle was nearly 40° and the three-dimensional boundary layer on the stationary cylinder relaxed quickly to a two-dimensional state. In order to determine the optimum size and location of the step, several experiments were carried out with and without rotation for various locations of these steps on the stationary cylinder. Two important criteria were adoptd to arrive at optimum values:

1. The step height should be sufficient to cause appreciable C_p-values before separation.

2. The streamwise location of the step on the stationary cylinder should be such that its influence on the flow field (i.e., the step-induced pressure field) decreases as the spinner is approached and, in fact, ideally becomes zero at the trailing edge of the spinner.

Figures 7 through 9 show the static-pressure data taken with and without rotation for different locations of the steps on the stationary cylinder. Figure 7 presents the static-pressure distribution for 12.7-mm and 25.4-mm steps at two locations. It is clear that the 25.4-mm step yields slightly higher C_p-values. Furthermore, because this step height is comparable to the thickness of the approaching boundary layer, it is expected to cause a strong perturbation of the boundary-layer flow (ref. 15). A strongly perturbed flow field is a challenging test case for the existing calculation methods and the associated turbulence models. For these reasons, 25.4-mm step was chosen as the optimum and used in all subsequent experiments.

Figure 8 compares the static-pressure distribution on the stationary cylinder without the step and with the 25.4-mm step located at $x = 306.4$ mm. It is very clearly seen in the figure that the influence of the step is asymptotically decreasing toward the spinner and is practically negligible at the end of the spinner. It should also be noticed that only after the first 150 mm of the stationary cylinder, the step influence becomes appreciable and both the pressure rise and pressure gradient become significant. However, as remarked earlier, the crossflow in the relaxing boundary layer is substantial only in the region very close to the beginning of the stationary cylinder (without step); it decays rapidly and the boundary layer returns to a two-dimensional state quickly. This region of substantial crossflow would therefore be little influenced by the pressure field caused by a 25.4-mm step at $x = 306.4$ mm. It is therefore apparent that this location of the

step is not close enough to the spinner to be considered a good choice. Figure 9 compares the static-pressure distribution on the stationary cylinder for different locations of the step. For clarity, only a few locations are included in the figure. Clearly, for reasons explained above, the step location at $x = 205$ mm is not satisfactory. On the other hand, the step locations at $x = 52.4$ mm and 103.2 mm are so close to the spinner that the influence of the step is certainly felt in the flow field over the spinner. From these distributions and those for other locations (not shown in the figure), it is concluded that $x = 154$ mm is the optimum choice for step location in terms of meeting the criterion stated earlier. All subsequent experiments, including LDV surveys, were therefore made with the 25.4-mm step located at $x = 154$ mm from the end of the spinner. It should be mentioned here that the conclusions regarding the optimum size and optimum location of step based on static-pressure surveys are supported by preliminary oil-flow visualization studies.

Finally, a few remarks on the nature of the step-induced pressure field and its comparison with the existing data are in order. Although a better appreciation of the pressure field would require a more closely spaced data near the step, the plots of figure 9 do clearly indicate the relaxing trend of the maximum pressure gradient just before separation. With the 25.4-mm step, a maxiumum C_p of 0.39 was reached very close to the step. The maximum pressure gradient (dC_p/dx) was 4.2/m, which is equivalent to, in wall coordinates,

$$p^+ = (\nu/\rho_\infty u_\tau^3)(dp/dx) \approx 1.09\times10^{-2}$$

The rotation seems to have a negligible influence on the pressure distribution, except for the fact that the pressure levels with rotation are slightly lower ahead of the step and slightly higher very close to the step. The pressure distributions are comparable to those obtained by Bradshaw and Galea (ref. 16) in their study of step-induced, two-dimensional separation of turbulent boundary layers. Their measured value of $C_{p,max}$ was 0.35.

Surface-Flow Direction

Surface-flow directions as estimated from oil-flow patterns obtained by placing oil dots of silicone fluid 200 (500 centistokes viscosity) along the top generator of the stationary cylinder are shown in figure 10. The direction can be estimated to within ±2°. Also shown for comparison are Higuchi's data taken from reference 12 (solid line). Considering the experimental uncertainty, the agreement between the present data and Higuchi's data for the case without the step is excellent. In the case of the flow with the step, it is very clear that the pressure gradient imposed by the step has a very strong influence on the flow, in that the otherwise relaxing flow is now continuously turning as it approaches the step. More discussion on this aspect appears below.

Figure 11 presents surface-flow directions as determined by a miniature, directional surface-fence gage. The accuracy of the direction measurement is ±1°. Also

included for comparison are Higuchi's fence data (refs. 11 and 14) and present oil-flow data. The solid line represents the prediction from a boundary-layer code which will be discussed later. It is seen that the agreement among the various data sets is very good, particularly for the flow without the step. The good agreement between the oil-flow data and the fence data for the flow with the step suggests that the calibration of the fence is unaffected by the adverse pressure gradient. With the step on the stationary cylinder, the relaxing flow behind the spinner is now subject to a step-induced, streamwise, adverse pressure gradient. The resulting streamwise deceleration reduces the streamwise-velocity component and the streamwise skin friction, but leaves the peripheral skin friction practically unaffected (see section below). This results in more turning of the flow as it approaches the step. At $x \approx 133$ mm (5.25 in.), the surface-flow direction is nearly 90°, implying that the streamwise component is zero. Farther downstream, this component is reversed in direction.

Wall Shear Stress

Figures 12 and 13 present skin-friction coefficients determined by the surface-fence gage. The overall accuracy of the data is estimated to be ±10%. The distribution of skin-friction coefficients on the stationary cylinder without the step is shown in figure 12. Also included for comparison are Higuchi's fence data (refs. 11 and 14). The solid lines represent predictions from a boundary-layer code which will be discussed later. It is to be noted that, in this investigation, the approaching boundary layer is slightly thicker and, therefore, lower levels of skin friction are expected. Considering this slightly thicker boundary layer and the experimental uncertainty in the data, the overall agreement between the present data and Higuchi's data is satisfactory for the relaxing region. Figure 13 compares the distribution of skin-friction coefficients measured with and without step and spin. It is clear that spinning increases skin friction except in the vicinity of separation. In other words, spinning may be considered to increase the eddy viscosity of the fluid. The streamwise pressure gradient induced by the step (see fig. 14) has a considerable effect on the streamwise skin-friction coefficient. The latter is reduced as the step is approached, goes through zero (the separation point), and reverses its sign close to the step. On the other hand, the peripheral skin friction remains practically unaffected by the pressure gradient until separation is approached. The separation point is estimated to be at $x = 133$ mm (5.25 in.) or 21 mm (0.83 in.) ahead of the step. The separation bubble is therefore a short one, being only 21 mm long.

Spin-Code Prediction

The spin code is basically an implicit, parabolic, marching method using a finite-difference scheme (see ref. 17). It can use different turbulence models ranging from a simple mixing-length model to a more complicated Reynolds-stress equation model. Higuchi and Rubesin (ref. 11) have compared the spin-code estimates with their experimental data for the relaxing boundary layer on the stationary

cylinder (without the step). The code prediction based on the Launder, Reece, and Rodi closure equation (see. ref. 18) for the turbulence model compared better with the data (without pressure gradient). These predictions are shown as solid lines in figures 11 and 12. Figures 15-17 show a comparison of the spin-code estimates with the present experimental data for the retarding boundary layer on the stationary cylinder with the 25.4-mm step located at $x = 154$ mm from the spinner. The estimates are based on the Launder, Reece, and Rodi closure equation for the turbulence model. It should be mentioned that the estimates shown here were obtained by running the spin code in the "cold start" mode, where the initial length of run (i.e., distance to the end of spinner) was determined by matching the computed momentum thicknesses in the axial and transverse directions to the experimentally determined values at the end of spin.

Before discussing the comparison, a few remarks on the limitations of the spin code are in order. It is a boundary-layer code and therefore needs an impressed pressure field as an input. It can handle only geometries with smooth curvature and attached flows and can go only as far as predicting incipient separation. Since this experimental configuration has an abrupt change in surface geometry at the location of the step and since the step-induced pressure gradient retards the boundary layer and ultimately makes it rapidly separate from the surface close to the step, the spin code cannot be expected to predict the complete boundary-layer development satisfactorily. However, with the right choice of the impressed pressure field as input to the code, it was possible to predict the development of the attached boundary layer up to the location of the separation. The following variants of the measured pressure distribution (see fig. 14) have been used in the spin code:

1. Experimental pressure distribution unmodified.

2. Experimental pressure distribution partly modified so that the pressure gradient existing just before the beginning of the plateau is extrapolated through the separated region. The extrapolation starts at $x = 125$ mm.

3. Experimental pressure distribution partly modified so that the maximum pressure gradient before the plateau is extrapolated through the separated region. The extrapolation starts at $x = 113$ mm.

Pressure variation across the boundary layer has been neglected. The use of extrapolated pressure distribution to calculate separation point was suggested by Cebeci et al. (ref. 19).

Figure 15 compares the distribution of measured skin friction coefficient in the absence of rotation with spin-code estimates. Over most of the attached flow region, the three predictions based on the above variants of measured pressure distribution do not differ from one another because the pressure field is unchanged and they are in good agreement with the experimental data. However, as the separation point is approached, they differ widely. The location of the incipient separation appears to be very sensitive to, and largely dependent upon, the type of pressure distribution extrapolated through the separated region. Thus, the

prediction based on pressure distribution (1) (above) yields local minimum and maximum values of C_f responding to the actual variations of static pressure through the separated region. The predictions based on pressure distributions (2) and (3) yield results that are closer to the measured data, the incipient separation point being slightly overestimated by the former and slightly underestimated by the latter.

Figure 16 compares with the distribution of streamwise and peripheral skin-friction coefficients with spin-code estimates. The comments made with reference to figure 15 are applicable also in the case of the streamwise coefficient, although the agreement between the prediction and the experiment is poorer. In the case of the peripheral skin-friction coefficient, all three predictions appear to be accurate up to the separation point, thus suggesting that the peripheral skin friction is insensitive to the type of axial pressure distribution.

Finally, figure 17 compares the measured surface flow direction with spin-code estimates. The comments made earlier with reference to figure 15 regarding spin-code predictions are applicable also to figure 17. As noted in figure 16, for $x < 50$ mm, the spin code slightly overpredicts both the peripheral skin friction and the streamwise skin friction. Since the surface-flow direction is the ratio of peripheral to streamwise skin friction, it is no surprise that the agreement between the prediction and the experimental data is improved for $x < 50$ mm, as shown in figure 17.

CONCLUSIONS

An experimental investigation of a swirling, axisymmetric, incompressible, turbulent boundary layer with and without a (step-induced) pressure gradient has been carried out. The surface-flow measurements included surface-pressure distribution and mean surface shear-stress vector and were supplemented by oil-flow visualization studies. Based on the analysis of the data and a comparison with spin-code prediction, the following conclusions are drawn:

1. The streamwise pressure gradient primarily influences only the streamwise component of skin friction, whereas the peripheral component remains relatively unaffected.

2. With extrapolated pressure distribution as input, the spin code based on the Launder, Reece, and Rodi closure equation for the Reynolds-stress model is able to predict the attached flow field and the location of the separation reasonably well.

REFERENCES

1. Chapman, D. R.: Computational Aerodynamics Development and Outlook, AIAA J., vol. 17, no. 12, Dec. 1979, pp. 1293-1313.

2. Marvin, J. G.: Turbulence Modeling for Computational Aerodynamics (Invited). AIAA Paper 82-0164, Orlando, FL, Jan. 1982.

3. Johnston, J. P.: Experimental Studies in Three-Dimensional Turbulent Boundary Layers, Report MD-34, Thermosciences Division, Stanford University, Stanford, CA, July 1976.

4. Bissonnette, L. R.; and Mellor, G. L.: Experiments on the Behavior of an Axisymmetric Turbulent Boundary Layer with a Sudden Circumferential Strain. J. Fluid Mech., vol. 63, part 2, 1974, pp. 369-413.

5. Furuya, Y.; Nakamura, I.; Yamashita, S.; and Ishii, T.: Experiments on the Relatively Thick Turbulent Boundary Layers on a Rotating Cylinder in Axial Flows (2nd Report, Flows under Pressure Gradients), Bulletin of the JSME, vol. 20, no. 140, Feb. 1977, pp. 191-200.

6. Arzoumanian, E.; Fulachier, L.; and Dumas, R.: Experimental Investigation of the Three-Dimensional Turbulent Boundary Layer on an Axially Rotated Cylinder, Second Symposium on Turbulent Shear Flows, London, England, July 2-4, 1979.

7. Nakamura, I.; and Yamashita, S.: Boundary Layers on Bodies of Revolution Spinning in Axial Flows. IUTAM Symposium on Three-Dimensional Turbulent Boundary Layers, Berlin, West Germany, March 29-April 1, 1982.

8. Elsenaar, A.; van den Berg, B.; and Lindhout, J. P. F.: Three-Dimensional Separation of Incompressible Turbulent Boundary Layer on an Infinite Swept Wing. Flow Separation, AGARD CP-168, 1975.

9. Hebbar, K. S.: An Experimental Investigation of the Near-Wall Region of a Three-Dimensional, Incompressible, Turbulent Boundary Layer Relaxing in a Zero Pressure Gradient. Ph.D Dissertation, University of Maryland, 1976, College Park, Maryland (University Microfilms No. 77-9513). (Also, J. Fluid Mech., Vol. 85, Part 1, March 1978, pp. 33-56 and AIAA J. Vol. 15, No. 10, Oct. 1977, pp. 1509-1511).

10. Fernholz, H. H.; and Vagt, J.-D.: Turbulence Measurements in an Adverse-Pressure Gradient Three-Dimensional Turbulent Boundary Layer along a Circular Cylinder. J. Fluid Mech., vol. 111, 1981, pp. 233-269.

11. Higuchi, H.; and Rubesin, M.: An Experimental and Computational Investigation of the Transport of Reynolds Stress in an Axisymmetric Swirling Boundary Layer. AIAA Paper 81-0416, St. Louis, MO, Jan. 1981.

12. Higuchi, H.: Relaxation of a Subsonic Swirling Turbulent Boundary-layer Flow, -- An Experimental Documentation of the Mean Flow Field Survey. Report DTN-8007-4, Dynamics Technology, Inc., Torrance, CA, Oct. 1980.

13. Driver, D. M.; and Hebbar, S. K.: Experimental Study of a Three-Dimensional, Shear Driven, Turbulent Boundary Layer Using a Three-Dimensional Laser Doppler Velocimeter. AIAA Paper 85-1610, Cincinnati, OH, July 1985.

14. Higuchi, H.: A Miniature, Directional, Surface Fence Gage for Three-Dimensional Turbulent Boundary Layer Measurements. AIAA Paper 83-1722, Danver, MA, July 1983.

15. Bradshaw, P.; and Wong, F. Y. F.: The Reattachment and Relaxation of a Turbulent Shear Layer. J. Fluid Mech., vol. 52, part 1, 1972, pp. 113-135.

16. Bradshaw, P.; and Galea, P. V.: Step-Induced Separation of a Turbulent Boundary Layer in Incompressible Flow. J. Fluid Mech., vol. 27, part 1, 1967, pp. 111-130.

17. Wilcox, D. C.: Recent Improvements to the Spinning Body Version of the "EDDYBL" Computer Program. Report DCW-R-24-01, DCW Industries, Inc., Studio City, CA, Nov. 1979.

18. Launder, B. E.; Reece, G. J.; and Rodi, W.: Progress in the Development of a Reynolds-Stress Turbulence Closure. J. Fluid Mech., vol. 68, part 3, 1975, pp. 537-566.

19. Cebeci, T.; Mosinskis, G. J.; and Smith, A. M. O.: Calculation of Separation Points in Incompressible Turbulent Flows. J. Aircraft, vol. 9, no. 9, Sept. 1972, pp. 618-624.

TABLE 1.- STATIC-PRESSURE DISTRIBUTION ON STATIONARY CYLINDER (WITHOUT STEP)

Distance, x		C_p	C_p
mm	in.	No spin	Spin
3.2	0.125	-0.0138	-0.0300
6.35	0.25	-0.0069	-0.0231
9.55	0.375	-0.0046	-0.0185
12.7	0.5	-0.0046	-0.0185
19	0.75	-0.0092	-0.0208
25.4	1	-0.0092	-0.0185
31.7	1.25	-0.0092	-0.0185
38	1.5	-0.0092	-0.0185
44.4	1.75	-0.0092	-0.0185
63.5	2.5	-0.0070	-0.0160
69.8	2.75	-0.0092	-0.0185
76	3.0	-0.0092	-0.0185
82.4	3.25	-0.0092	-0.0185
89	3.5	-0.0092	-0.0185
95.3	3.75	-0.0092	-0.0185
101.6	4	-0.0092	-0.0185
114.3	4.5	-0.0092	-0.0185
127	5	-0.0092	-0.0185
139.7	5.5	-0.0092	-0.0185
152.4	6	-0.0092	-0.0185
165.1	6.5	-0.0092	-0.0185
177.8	7	-0.0092	-0.0185
190.5	7.5	-0.0092	-0.0185
203.2	8	-0.0092	-0.0185
215.9	8.5	-0.0092	-0.0185
228.6	9	-0.0092	-0.0185
254.0	10	-0.0092	-0.0185
279.4	11	-0.0092	-0.0139
304.8	12	-0.0092	-0.0185
355.6	14	-0.0092	-0.0185
381.0	15	-0.0092	-0.0185
406.4	16	-0.0092	-0.0185
431.8	17	-0.0092	-0.0185
457.2	18	-0.0046	-0.0139
482.6	19	-0.0092	-0.0139
508.0	20	-0.0092	-0.0185
533.4	21	-0.0115	-0.0185
558.8	22	-0.0138	-0.0231
584.2	23	-0.0183	-0.0278
609.6	24	-0.0229	-0.0278

TABLE 2.- STATIC-PRESSURE DISTRIBUTION ON STATIONARY CYLINDER FOR TWO LOCATIONS OF 12.7-mm STEP

Distance, x		Step at x = 154 mm		Step at x = 306.4 mm	
		C_p	C_p	C_p	C_p
mm	in.	No spin	Spin	No spin	Spin
3.2	0.125	0	-0.0141	0.0046	-0.0230
6.35	0.25	0.0093	-0.0094	0.0092	-0.0138
9.55	0.375	0.0116	-0.0047	0.0115	-0.0092
12.7	0.5	0.0139	-0.0047	0.0115	-0.0092
19	0.75	0.0139	-0.0047	0.0092	-0.0138
25.4	1	0.0139	0.0000	0.0092	-0.0138
31.7	1.25	0.0139	0.0000	0.0092	-0.0138
38	1.5	0.0186	0.0047	0.0092	-0.0138
44.4	1.75	0.0232	0.0094	0.0092	-0.0092
63.5	2.5	0.0442	0.0282	0.0092	-0.0092
69.8	2.75	0.0512	0.0376	0.0092	-0.0092
76	3	0.0558	0.0446	0.0092	-0.0092
82.4	3.25	0.0651	0.0516	0.0092	-0.0046
89	3.5	0.0791	0.0657	0.0092	-0.0092
95.3	3.75	0.0930	0.0798	0.0092	-0.0092
101.6	4	0.1116	0.0986	0.0092	-0.0092
114.3	4.5	0.1674	0.1549	0.0092	-0.0092
127	5	0.2372	0.2535	0.0092	-0.0092
139.7	5.5	0.3023	0.3239	0.0138	-0.0046
152.4	6	0.3535	0.3615	0.0138	0.0000
165.1	6.5	---	---	0.0138	0.0000
177.8	7	---	---	0.0138	0.0046
190.5	7.5	---	---	0.0183	0.0092
203.2	8	---	---	0.0229	0.0184
215.9	8.5	---	---	0.0367	0.0276
228.6	9	---	---	0.0550	0.0415
254.0	10	---	---	0.1101	0.1014
279.4	11	---	---	0.2339	0.2350
304.8	12	---	---	0.3670	0.3641

TABLE 3a.- STATIC-PRESSURE DISTRIBUTION ON STATIONARY CYLINDER FOR DIFFERENT LOCATIONS OF 25.4-mm STEP

Distance, x		Step at x = 52.4 mm		Step at x = 77.6 mm		Step at x = 103.2 mm		Step at x = 115.9 mm	
mm	in.	C_p No spin	C_p Spin	C_p No spin	C_p Spin	C_p No spin	C_p Spin	C_p No spin	C_p Spin
3.2	0.125	0.2340	0.2279	0.1403	0.1087	0.0722	0.0514	0.0562	0.0371
6.35	0.25	0.2490	0.2447	0.1530	0.1251	0.0827	0.0564	0.0664	0.0473
9.55	0.375	0.2715	0.2651	0.1637	0.1400	0.0909	0.0643	0.0713	0.0538
12.7	0.5	0.2872	0.2923	0.1753	0.1520	0.0911	0.0716	0.0762	0.0567
19	0.75	0.3062	0.3304	0.2025	0.1800	0.1101	0.0872	0.0853	0.0663
25.4	1	0.3255	0.3674	0.2342	0.2145	0.1239	0.1063	0.0959	0.0779
31.7	1.25	0.3373	0.3836	0.2653	0.2528	0.1473	0.1253	0.1120	0.0925
38	1.5	0.3336	0.3900	0.2956	0.2967	0.1748	0.1522	0.1305	0.1108
44.4	1.75	0.3156	0.3837	0.3189	0.3393	0.2055	0.1825	0.1528	0.1312
63.5	2.5	---	---	0.3383	0.3855	0.2981	0.2967	0.2369	0.2206
69.8	2.75	---	---	0.3252	0.3778	0.3231	0.3351	0.2684	0.2572
76	3	---	---	0.4119	0.4207	0.3301	0.3615	0.2969	0.2953
82.4	3.25	---	---	---	---	0.3432	0.3816	0.3201	0.3321
89	3.5	---	---	---	---	0.3437	0.3843	0.3367	0.3579
95.3	3.75	---	---	---	---	0.3266	0.3827	0.3448	0.3774
101.6	4	---	---	---	---	0.4117	0.4207	0.3476	0.3820
114.3	4.5	---	---	---	---	---	---	0.4096	0.4219

TABLE 3b.- STATIC-PRESSURE DISTRIBUTION ON STATIONARY CYLINDER FOR DIFFERENT LOCATIONS OF 25.4-mm STEP

Distance, x		Step at x = 128.6 mm		Step at x = 154 mm		Step at x = 204.8 mm		Step at x = 306.4 mm	
mm	in.	C_p No spin	C_p Spin	C_p No spin	C_p Spin	C_p No spin	C_p Spin	C_p No spin	C_p Spin
3.2	0.125	0.0360	0.0210	0.0251	0.0075	0.0099	-0.0141	0.0047	-0.0118
6.35	0.25	0.0458	0.0318	0.0295	0.0155	0.0027	-0.0138	0.0094	-0.0047
9.55	0.375	0.0508	0.0386	0.0340	0.0165	0.0040	-0.0120	0.0118	-0.0047
12.7	0.5	0.0539	0.0407	0.0367	0.0194	0.0171	-0.0081	0.0118	-0.0047
19	0.75	0.0606	0.0461	0.0389	0.0224	0.0161	0.0074	0.0118	-0.0047
25.4	1	0.0694	0.0525	0.0409	0.0255	0.0146	0.0084	0.0118	-0.0047
31.7	1.25	0.0788	0.0632	0.0457	0.0313	0.0152	0.0016	0.0118	-0.0047
38	1.5	0.0922	0.0754	0.0525	0.0378	0.0219	-0.0031	0.0118	-0.0024
44.4	1.75	0.1100	0.0912	0.0627	0.0486	0.0266	0.0127	0.0150	0.0000
63.5	2.5	0.1768	0.1616	0.1031	0.0870	0.0310	0.0321	0.0165	0.0047
69.8	2.75	0.2052	0.1858	0.1187	0.1015	0 0347	0.0347	0.0165	0.0047
76	3	0.2336	0.2175	0.1396	0.1183	0.0301	0.0359	0.0165	0.0047
82.4	3.25	0.2633	0.2577	0.1605	0.1362	0.0377	0.0339	0.0165	0.0047
89	3.5	0.2918	0.2895	0.1817	0.1642	0.0408	0.0393	0.0165	0.0047
95.3	3.75	0.3205	0.3348	0.2131	0.1935	0.0482	0.0444	0.0165	0.0047
101.6	4	0.3339	0.3606	0.2418	0.2232	0.0578	0.0566	0.0165	0.0047
114.3	4.5	0.3469	0.3763	0.3028	0.3031	0.0872	0.0782	0.0189	0.0047
127	5	0.4149	0.4194	0.3385	0.3572	0.1248	0.1112	0.0236	0.0094
139.7	5.5	---	---	0.3405	0.3772	0.1715	0.1576	0.0259	0.0142
152.4	6	---	---	0.3923	0.4086	0.2285	0.2186	0.0307	0.0189
165.1	6.5	---	---	---	---	0.2916	0.2988	0.0377	0.0237
177.8	7	---	---	---	---	0.3269	0.3563	0.0472	0.0332
190.5	7.5	---	---	---	---	0.3400	0.3725	0.0590	0.0450
203.2	8	---	---	---	---	0.4047	0.4049	0.0755	0.0640
215.9	8.5	---	---	---	---	---	---	0.0991	0.0877
228.6	9	---	---	---	---	---	---	0.1321	0.1185
254.0	10	---	---	---	---	---	---	0.2406	0.2227
279.4	11	---	---	---	---	---	---	0.3349	0.3507
304.8	12	---	---	---	---	---	---	0.3962	0.3981

TABLE 4.- SKIN-FRICTION DATA ON STATIONARY CYLINDER (WITHOUT STEP) OBTAINED FROM SURFACE-FENCE GAGE

Distance, x		No spin	With spin		
mm	in.	$C_{fx} \times 10^3$	$C_{fx} \times 10^3$	$C_{fz} \times 10^3$	β_w, deg
6.35	0.25	3.50	3.93	2.42	31.6
12.7	0.5	3.01	3.59	1.68	25.1
19	0.75	3.04	3.31	1.38	22.6
25.4	1	2.97	3.48	1.38	21.7
38	1.5	3.09	3.54	1.25	19.4
76	3	3.00	3.62	0.87	13.4
89	3.5	3.04	3.69	0.75	11.5
101.6	4	3.03	3.56	0.68	10.8
127	5	3.03	3.47	0.54	8.9
152.4	6	2.98	3.32	0.51	8.7
203.2	8	2.92	3.20	0.41	7.3
304.8	12	2.93	3.14	0.30	5.4
406.4	16	2.97	3.08	0.24	4.4
508	20	3.18	3.31	0.23	4.0
609.6	24	3.12	3.23	0.19	3.4

TABLE 5.- SKIN-FRICTION DATA ON STATIONARY CYLINDER (WITH 25.4-mm STEP LOCATED AT x = 154 mm) OBTAINED FROM SURFACE-FENCE GAGE

Distance, x		No spin	With spin		
mm	in.	$C_{fx} \times 10^3$	$C_{fx} \times 10^3$	$C_{fz} \times 10^3$	β_w, deg
6.35	0.25	3.32	3.66	2.34	32.7
12.7	0.50	2.82	3.32	1.72	27.4
19	0.75	2.75	3.01	1.32	23.7
25.4	1	2.74	3.10	1.29	22.6
38	1.5	2.65	3.17	1.21	21.0
76	3	2.12	2.69	0.81	16.7
89	3.5	1.71	2.36	0.75	17.5
101.6	4	1.17	1.74	0.68	21.4
127	5	0.30	0.36	0.47	52.4
152.4	6	-1.30	-1.25	0.21	-9.37

TABLE 6.- SURFACE-FLOW ANGLE DATA ON STATIONARY CYLINDER OBTAINED FROM OIL-FLOW PATTERNS

Distance, x		Surface flow angle β_w, in deg	
mm	in.	No step	25.4-m step at x = 154 mm
3.2	0.125	37.5	38.5
6.35	0.25	32	33
12.7	0.5	25	27
19	0.75	23	25
25.4	1	20	23
38	1.5	18	20
50.8	2	16	17
63.5	2.5	14	15
76	3	---	18
89	3.5	12	21
101.6	4	10	25
114.3	4.5	9	40
127	5	8	60
133.3	5.25	---	≈90
139.7	5.5	---	-75 (reverse flow)
152.4	6	7	-11 (reverse flow)
203.2	8	6.5	---
254.0	10	6	---
304.8	12	5.5	---
406.4	16	4.5	---
508	20	---	---
609.6	24	3.5	---

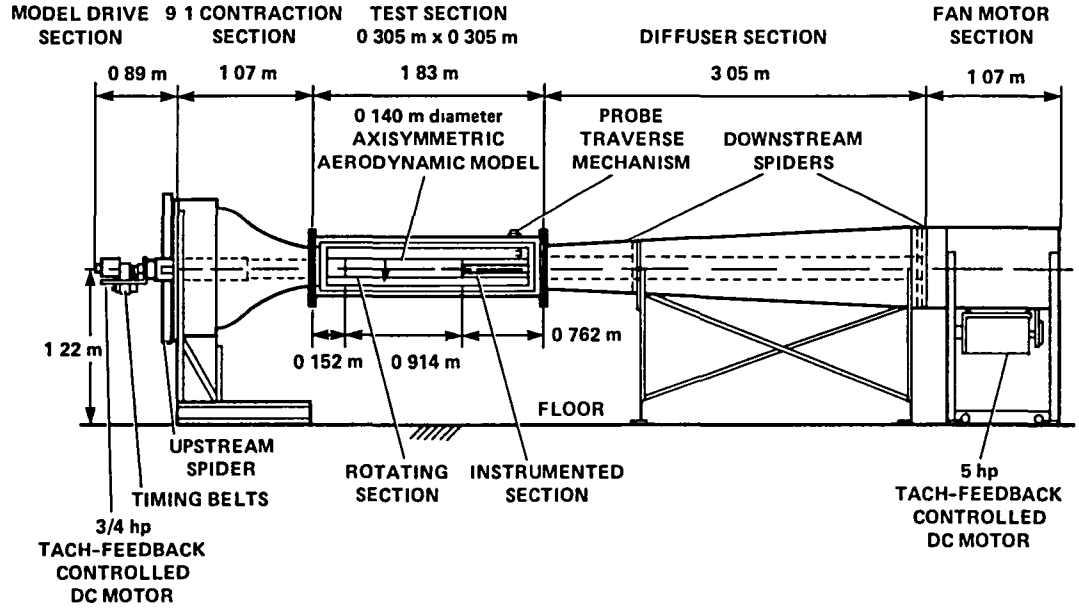

a) LOW SPEED WIND TUNNEL

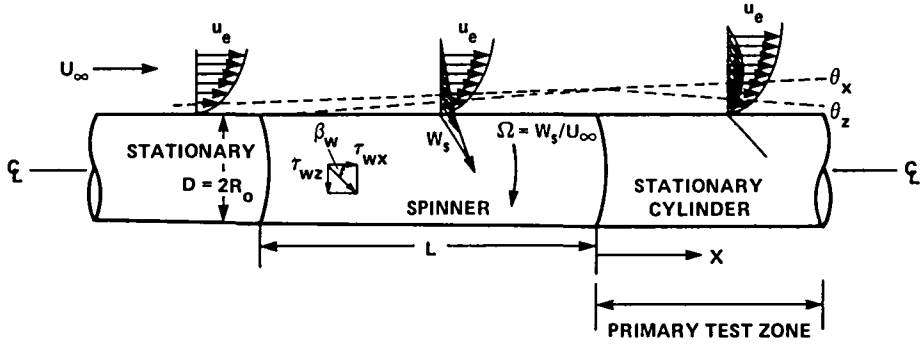

$U_\infty = W_s = 36\ 3$ m/s, D = 0 140 m, L = 0 914 m, $\delta \sim 2\ 5$ cm AT x = 0

b) BASIC FLOW CONFIGURATION

Figure 1.- Experimental arrangement.

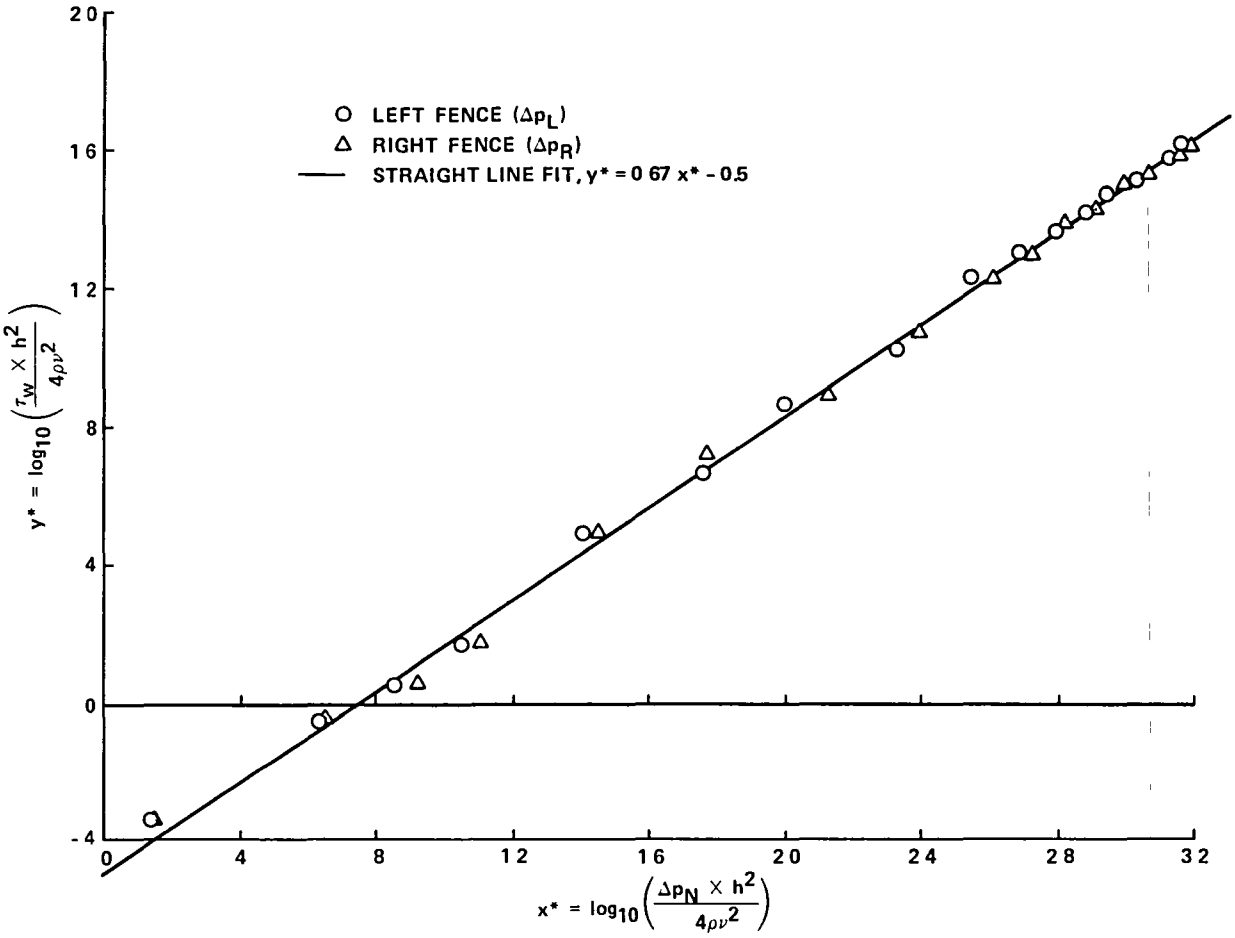

Figure 2.- Magnitude calibration of surface-fence-gage elements.

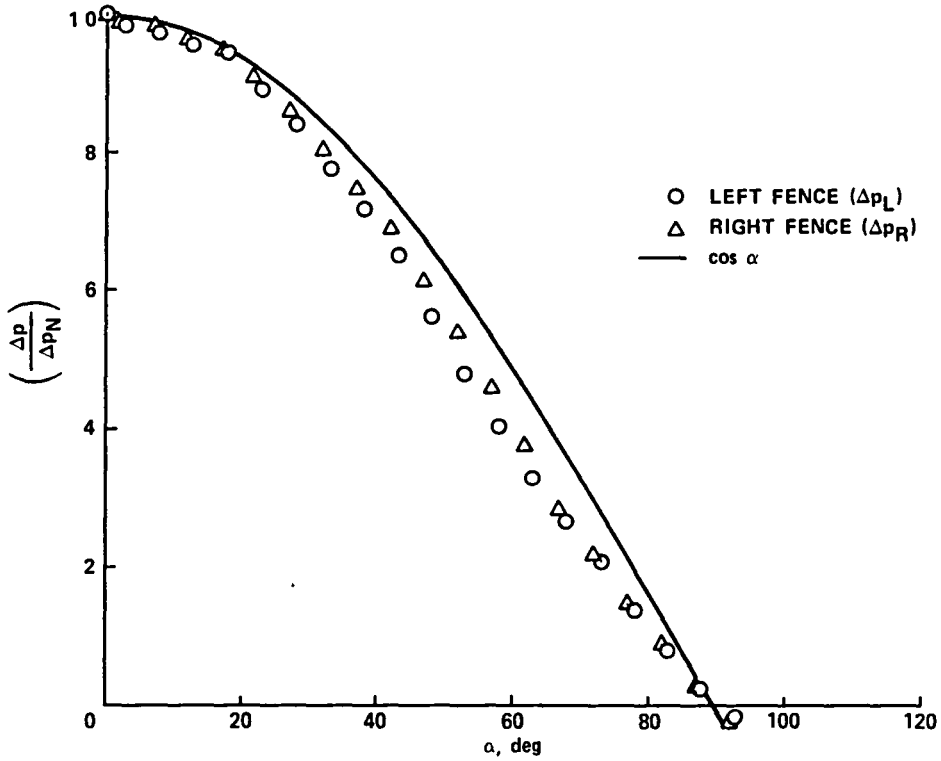

Figure 3.- Yaw characteristics of surface-fence-gage elements.

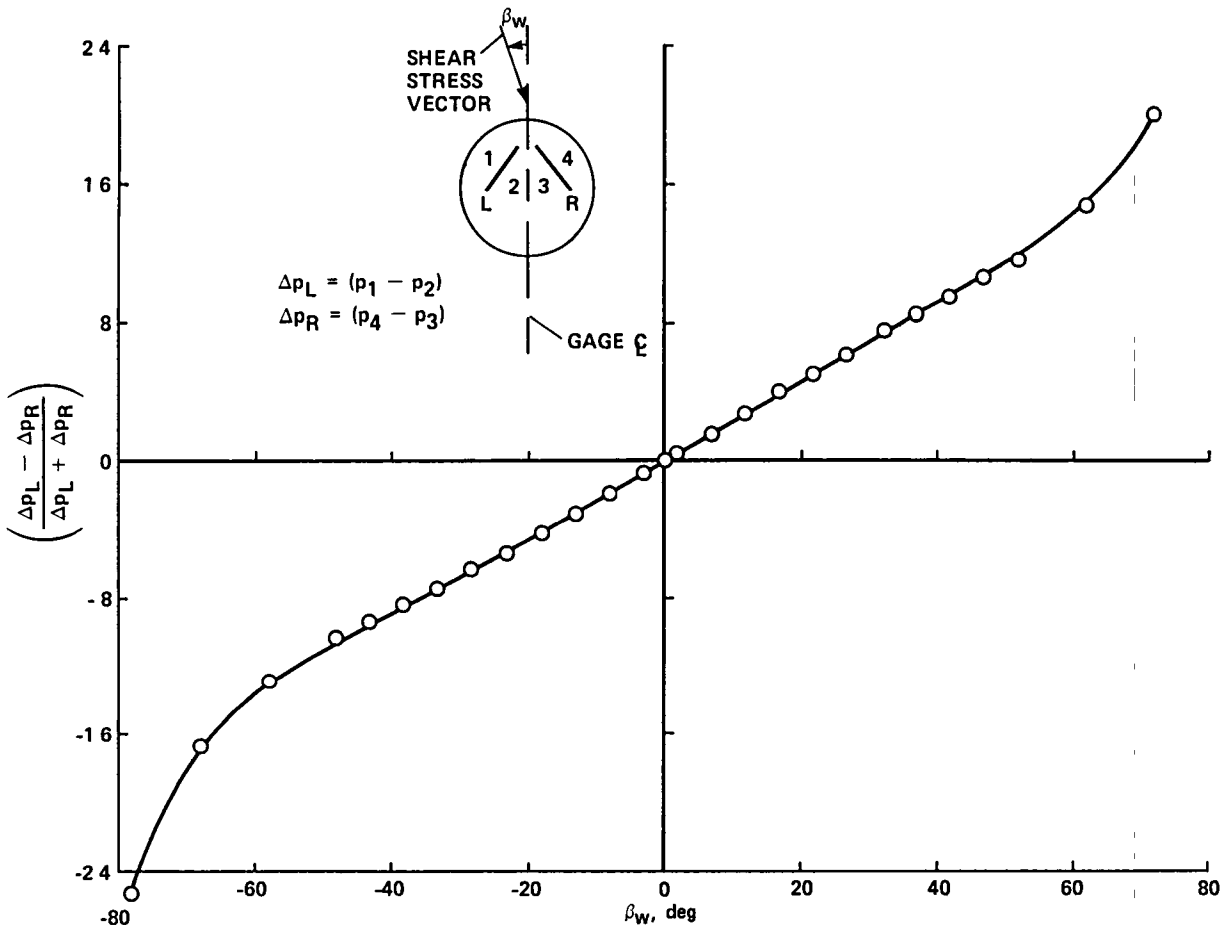

Figure 4.- Directional calibration of surface-fence gage.

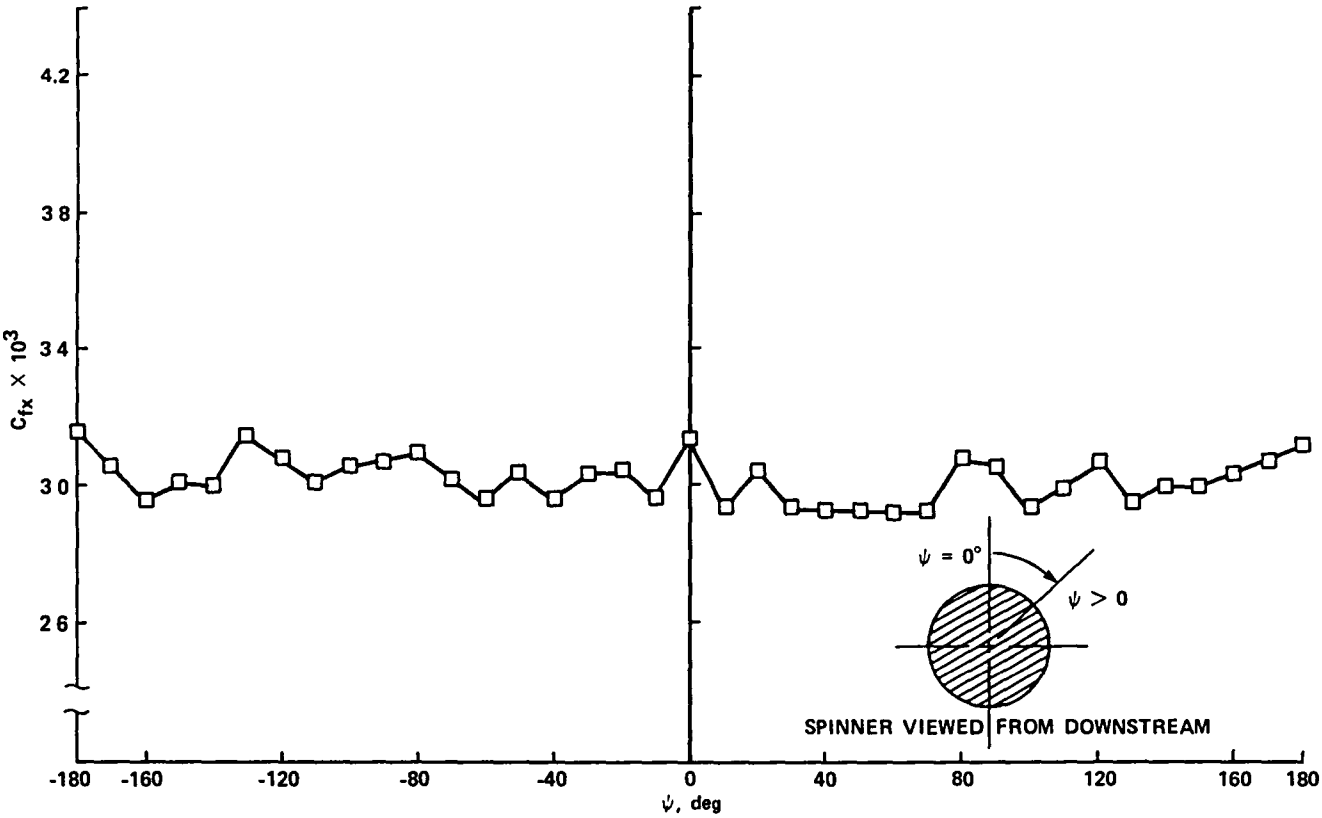

Figure 5.- Preston tube axisymmetry check of the boundary layer on the stationary spinner at x = -102 mm.

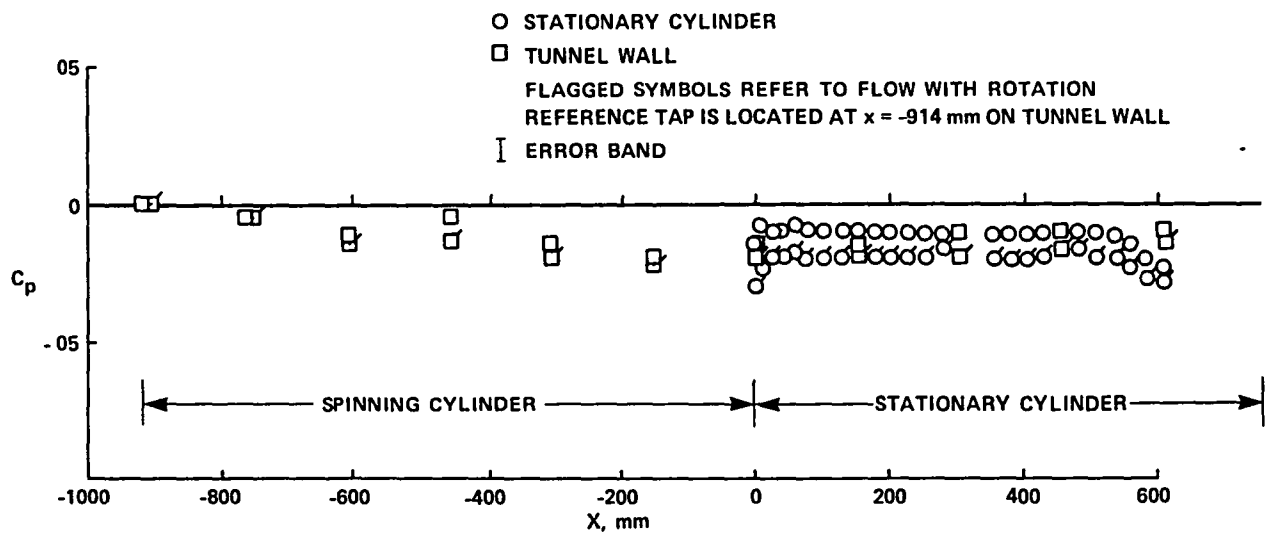

Figure 6.- Static-pressure variation in the test section.

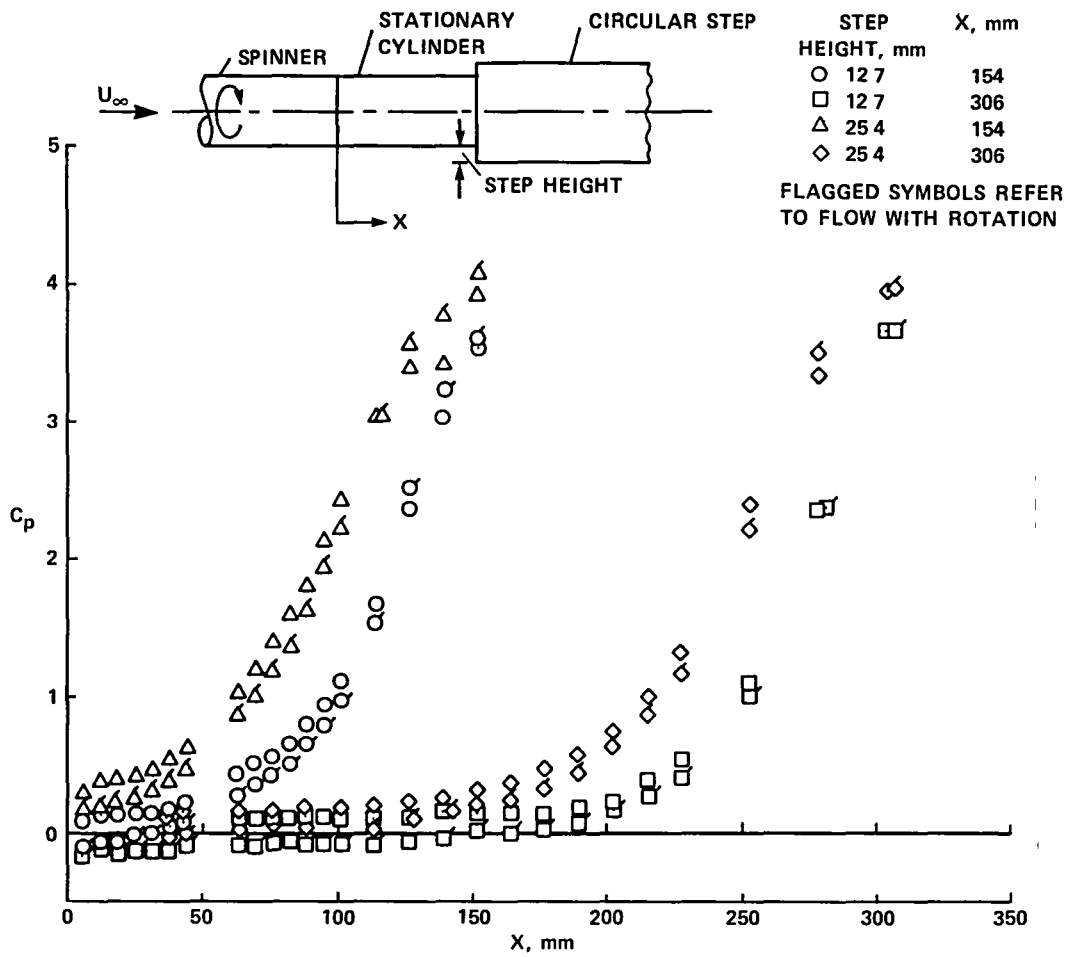

Figure 7.- Static-pressure distribution on stationary cylinder for different step heights.

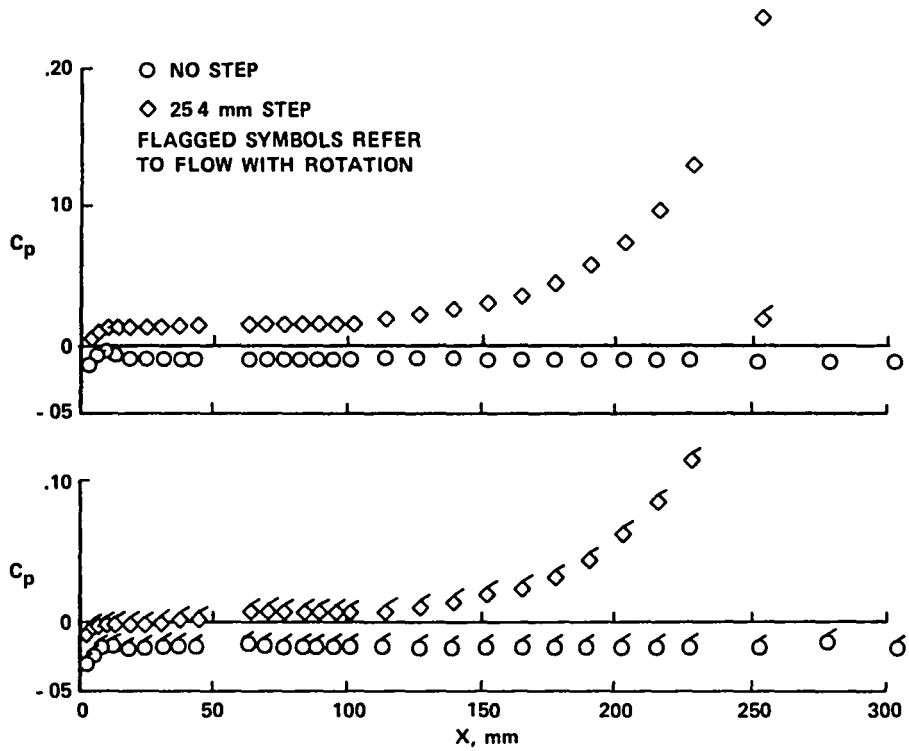

Figure 8.- Static-pressure distribution on stationary cylinder without step and with 25.4-mm step located at x = 306 mm from spinner.

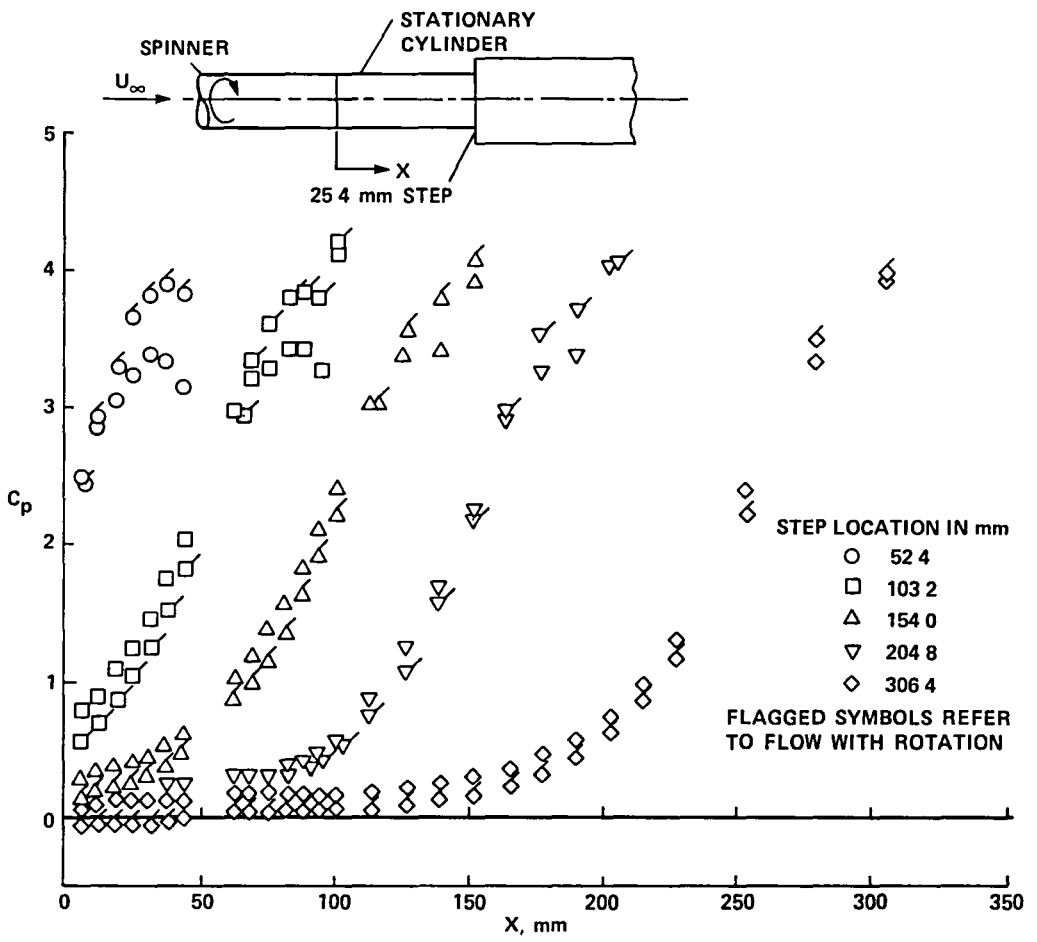

Figure 9.- Static-pressure distribution on stationary cylinder for different locations of 25.4-mm step.

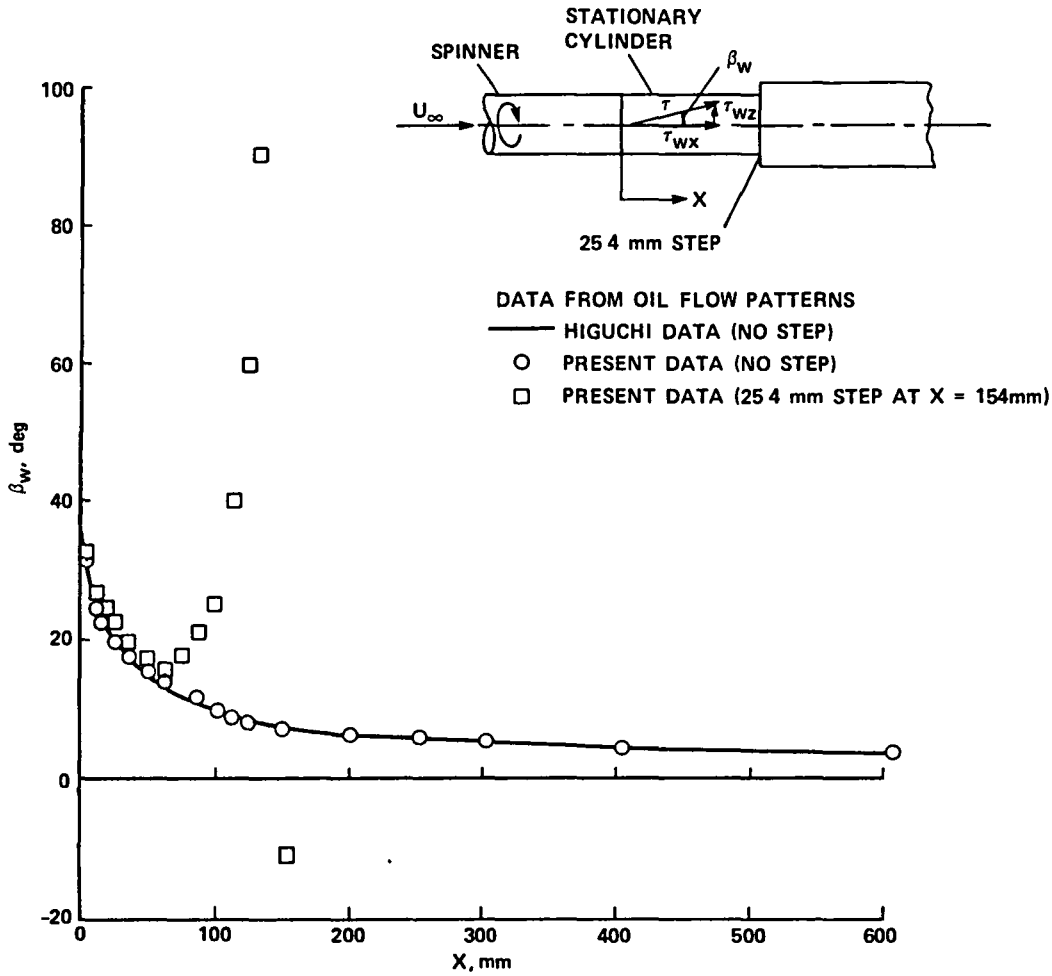

Figure 10.- Surface-flow direction on stationary cylinder without step and with 25.4-mm step located at x = 154 mm from spinner.

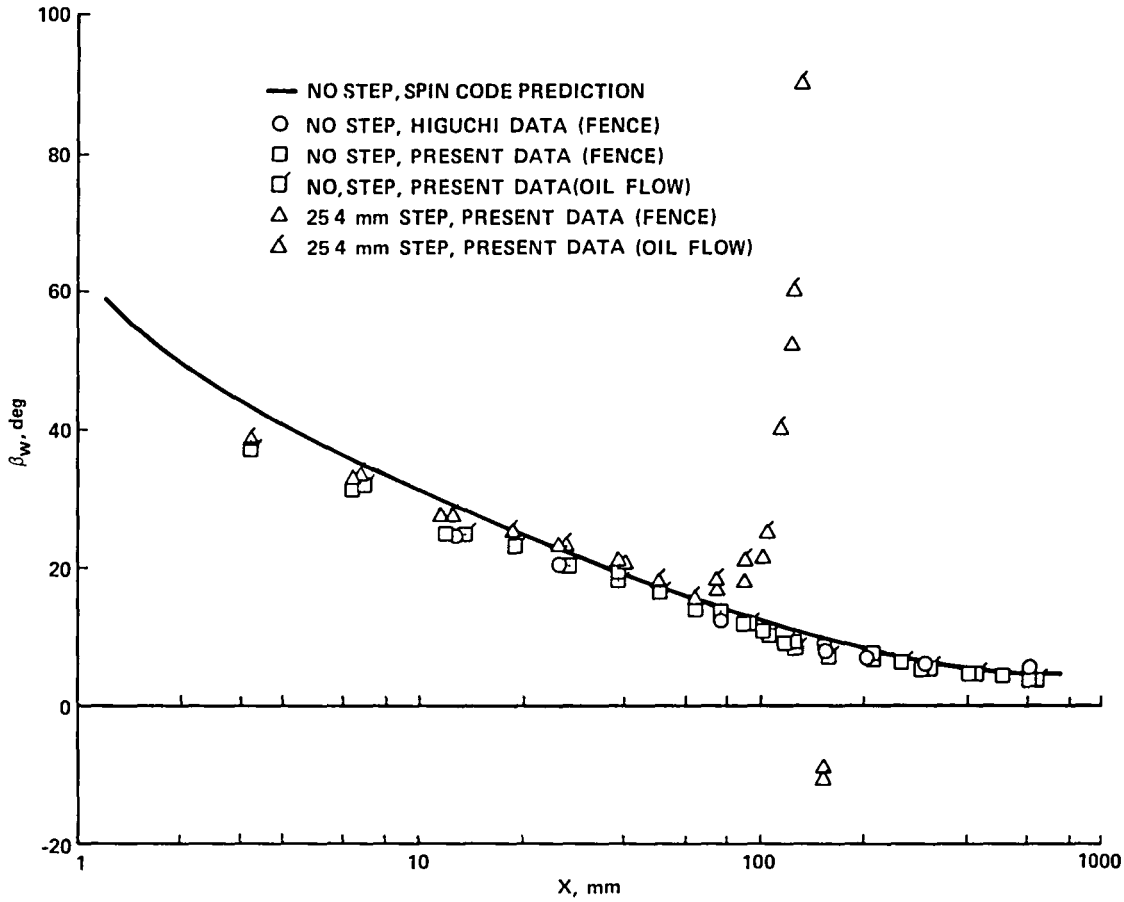

Figure 11.- Surface-flow direction on stationary cylinder without step and with 25.4-mm step located at x = 154 mm from spinner.

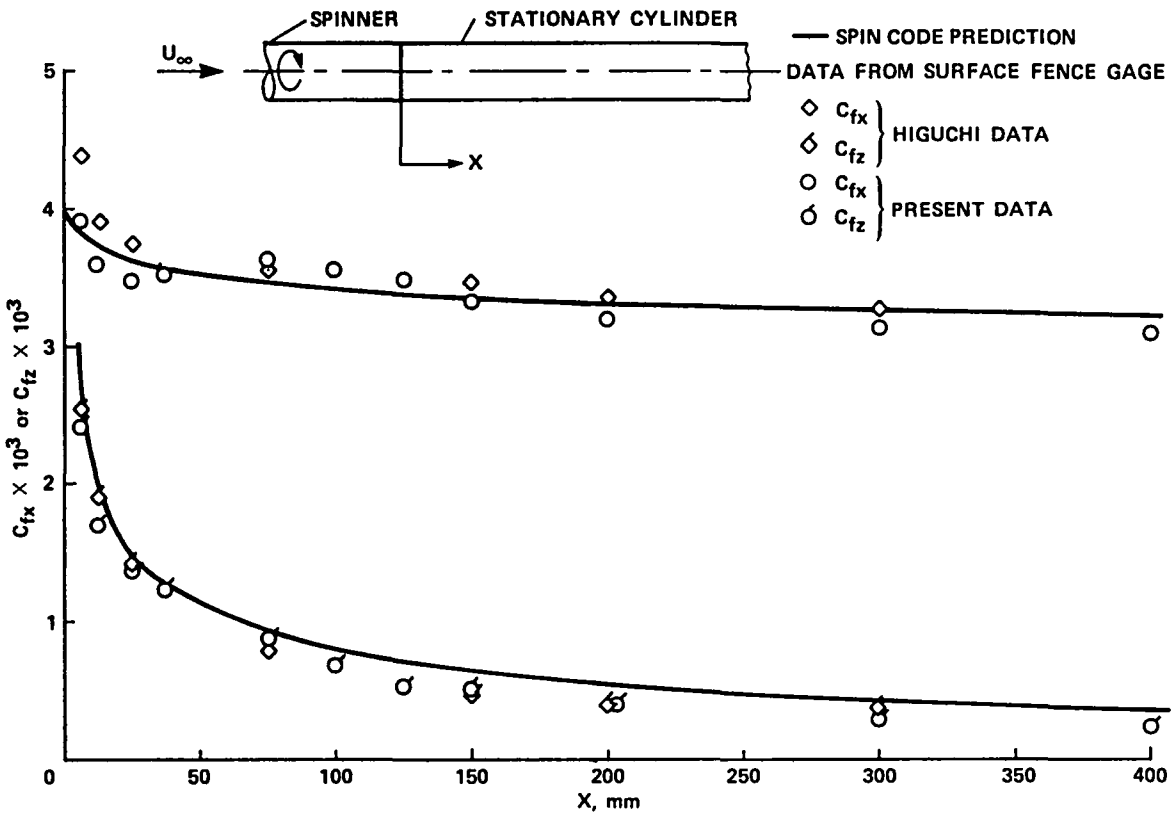

Figure 12.- Skin-friction coefficients on stationary cylinder without step.

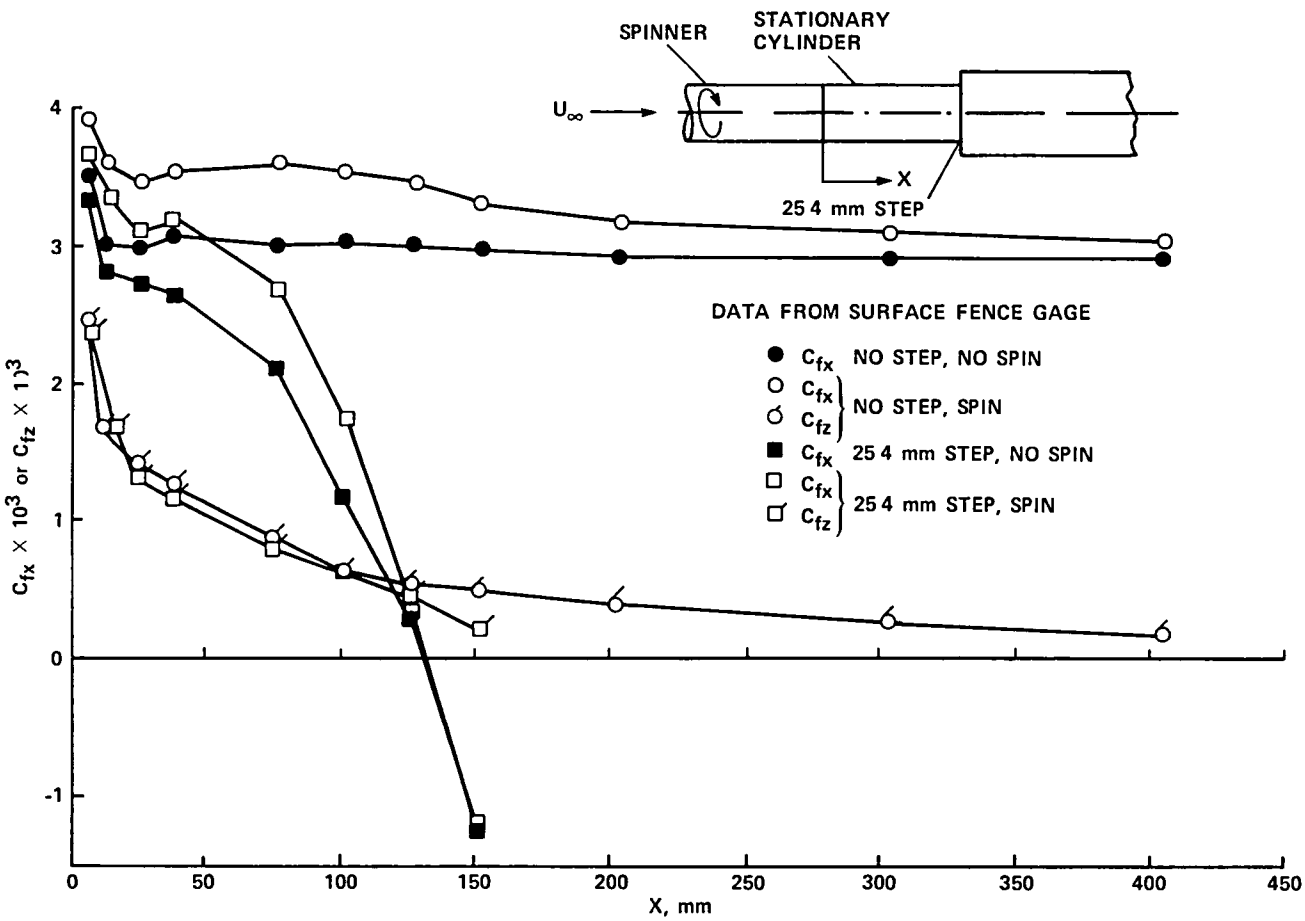

Figure 13.- Skin-friction on stationary cylinder without step and with 25.4-mm step located at x = 154 mm from spinner.

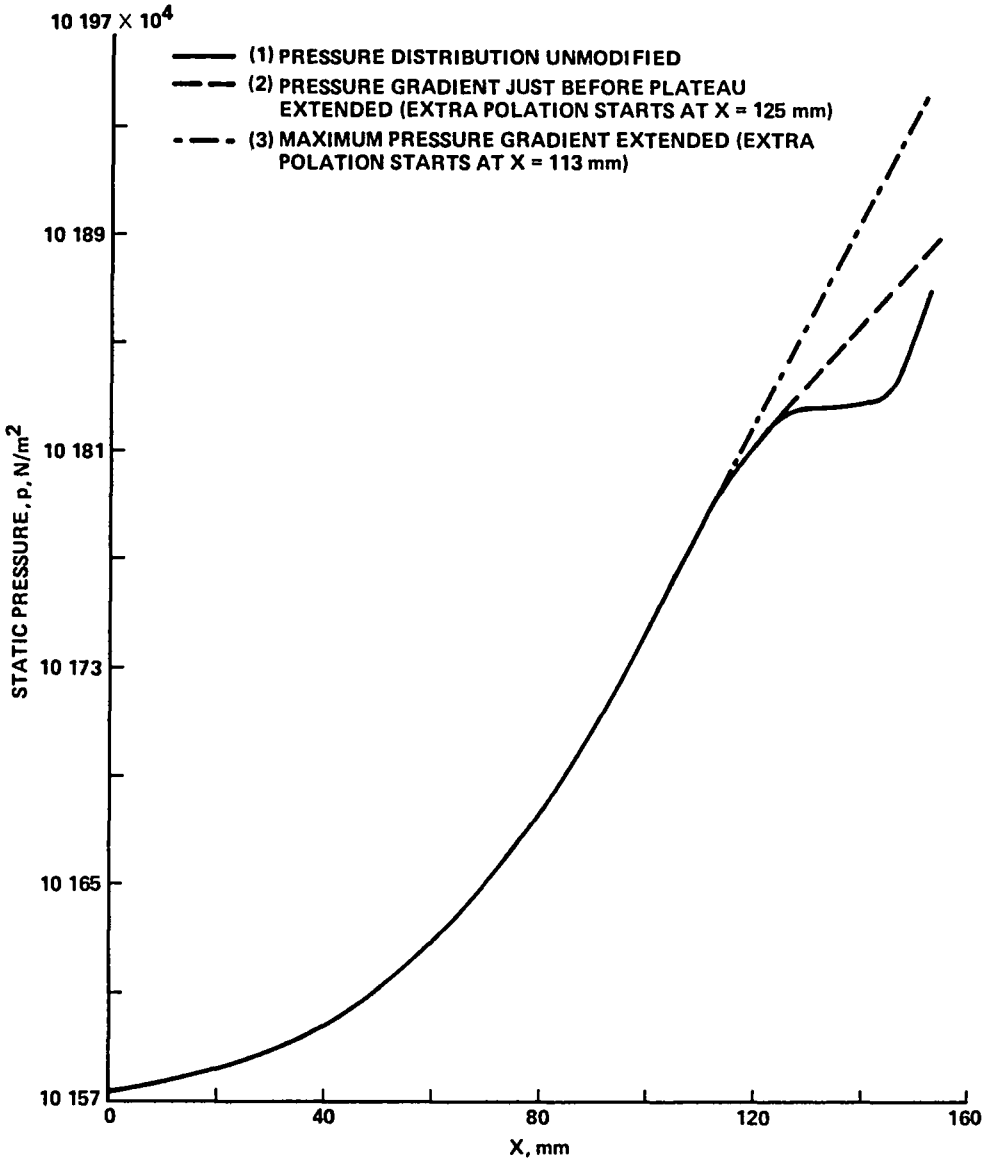

Figure 14.- Measured and extrapolated pressure distributions on stationary cylinder (with 25.4-mm step located at x = 154 mm from spinner and without rotation) used as input to the spin code.

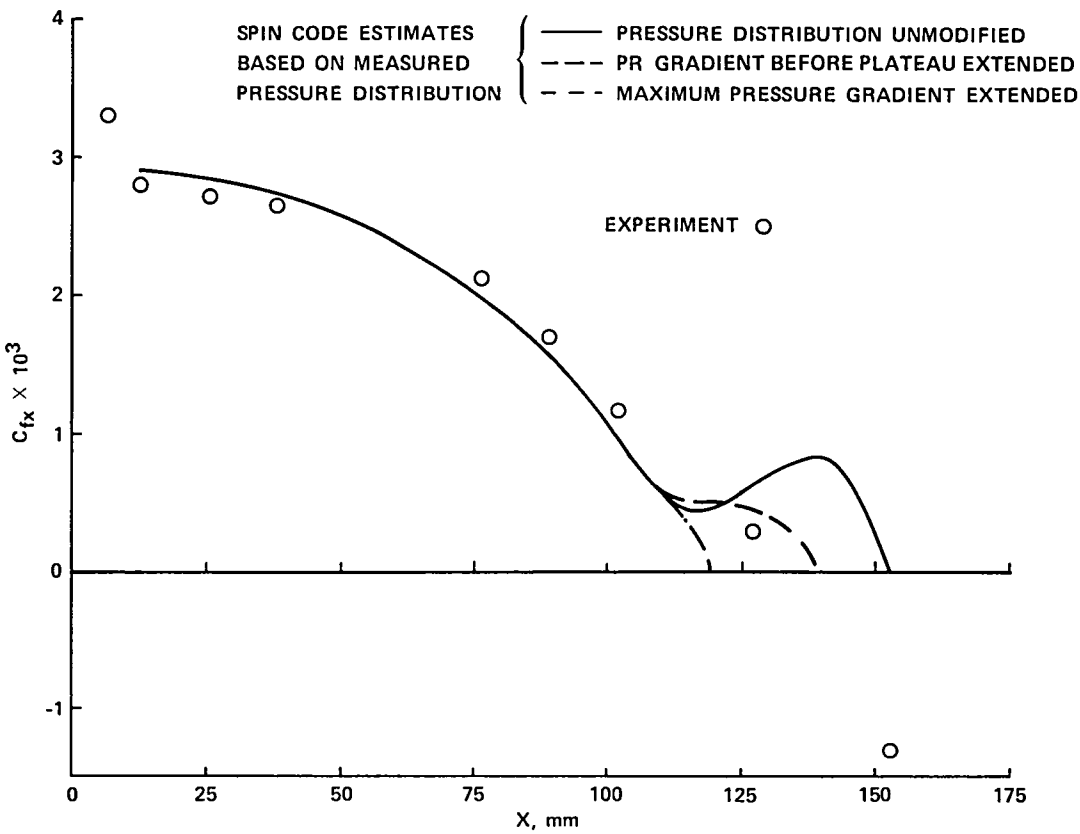

Figure 15.- Comparison between experimental data and spin-code estimates of skin friction based on measured pressure distribution without spin and with 25.4-mm step located at x = 154 mm from spinner.

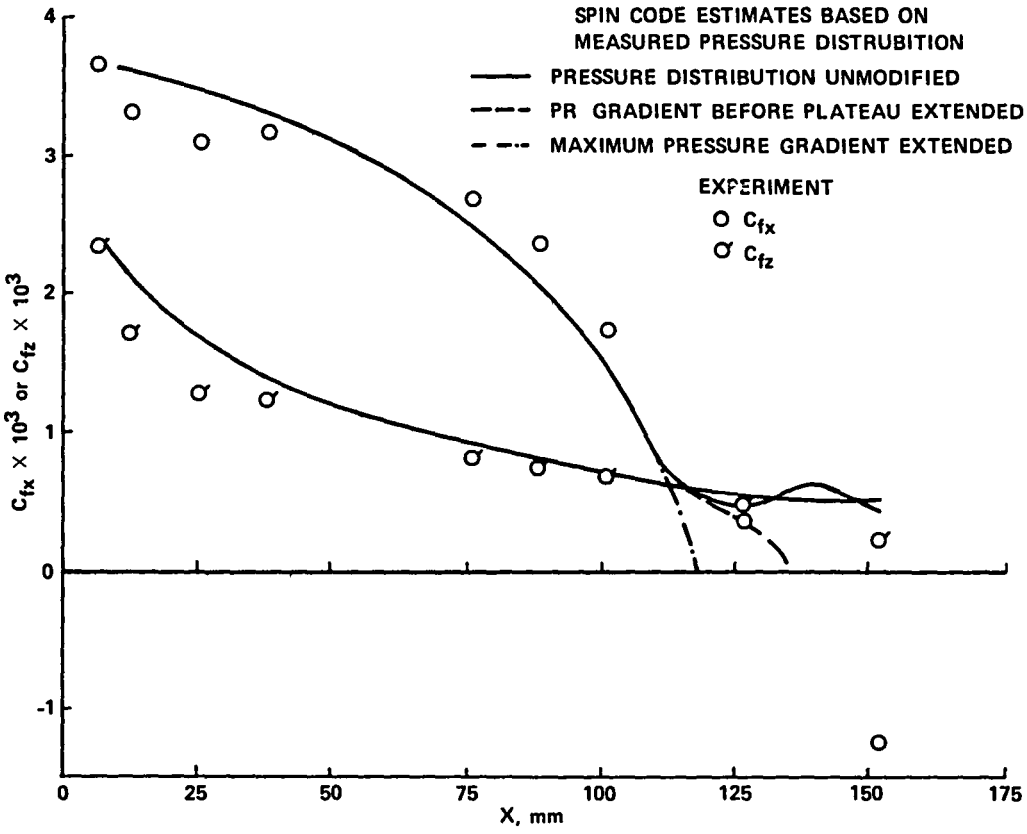

Figure 16.- Comparison between experimental data and spin-code estimates of skin frictions based on measured pressure distribution with 25.4-mm step located at x = 154 mm from spinner.

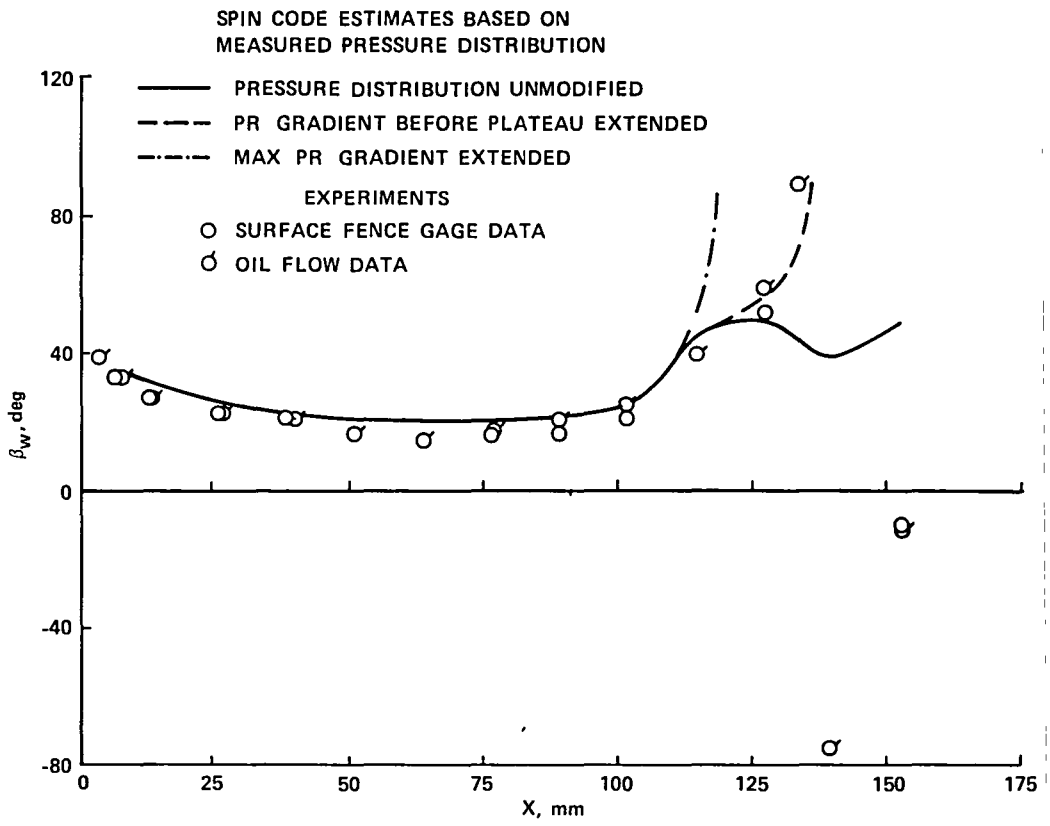

Figure 17.- Comparison between experimental data and spin-code estimates of surface-flow direction based on measured pressure distribution with 25.4-mm step located at x = 154 mm from spinner.

1 Report No	2 Government Accession No	3 Recipient's Catalog No
NASA TM-86768		

4 Title and Subtitle	5 Report Date
A THREE-DIMENSIONAL TURBULENT BOUNDARY LAYER UNDERGOING TRANSVERSE STRAIN AND STREAMWISE PRESSURE GRADIENT	August 1985
	6 Performing Organization Code

7 Author(s)	8 Performing Organization Report No
Sheshagiri K. Hebbar, Senior NRC Research Associate, and David M. Driver	85323
	10 Work Unit No
	505-31-01
9 Performing Organization Name and Address	11 Contract or Grant No
Ames Research Center Moffett Field, CA 94035	
	13 Type of Report and Period Covered
12 Sponsoring Agency Name and Address	Technical Memorandum
National Aeronautics and Space Administration Washington, D.C. 20546	14 Sponsoring Agency Code

15 Supplementary Notes

Point of contact: D. M. Driver, Ames Research Center, MS 229-1, Moffett Field, CA 94035. (415) 694-6156 or FTS 464-6156

16 Abstract

Results from an experimental investigation designed to provide data on both mean and turbulence quantities in the axisymmetric, swirling boundary layer (with and without pressure gradient) flowing over a stationary cylinder downstream of a spinning cylindrical section are presented. The pressure gradient was introduced into the flow field by a 25.4-mm-high, forward-facing, circular step mounted on the stationary cylinder, the step height being nearly equal to the thickness of the approaching boundary layer. All the measurements were made at a nominal upstream reference Reynolds number of 2.4×10^6/m (corresponding to an upstream reference velocity of 36-37 m/sec) with the rotation of the spinner set to make its peripheral speed equal the reference velocity. The data reported include measurements of surface pressure and the mean surface shear-stress vector taken with a miniature, directional, surface-fence gage. These measurements were supplemented by oil-flow visualization studies of the stationary cylinder. The data indicate that the streamwise pressure gradient controls the development of the streamwise component of wall shear, but leaves the peripheral component of wall shear practically unaffected. Comparison of the data with predictions from a boundary-layer computer code, using a Reynolds-stress equation model and a slightly modified, experimental pressure distribution, shows that it is possible to predict the attached flow field and the location of the separation reasonably well.

17 Key Words (Suggested by Author(s))	18 Distribution Statement
Three-dimensional boundary layer Skin friction Pressure gradient Transverse strain Turbulence model	Unlimited Subject category - 34

19 Security Classif (of this report)	20 Security Classif (of this page)	21 No of Pages	22 Price*
Unclassified	Unclassified	38	A03

*For sale by the National Technical Information Service, Springfield, Virginia 22161

End of Document